

# Mapping H<sub>2</sub> Excitation and Mass across M51 with the Spitzer Infrared Spectrograph

Gregory Brunner<sup>1,2</sup>

Department of Physics and Astronomy, Rice University,  
Houston, TX 77005

gbrunner@ipac.caltech.edu, gbrunner@rice.edu

Kartik Sheth<sup>3</sup>, Lee Armus<sup>3</sup>, and George Helou<sup>3</sup>

Spitzer Science Center, Pasadena, CA 91125

Eva Schinnerer<sup>4</sup>

Max-Planck-Institüt für Astronomie, Heidelberg, Germany

Stuart Vogel<sup>5</sup> and Mark Wolfire<sup>5</sup>

Department of Astronomy, University of Maryland, College Park, MD 20741

and

Reginald Dufour<sup>1</sup>

Department of Physics and Astronomy, Rice University, Houston, TX 77005

Received \_\_\_\_\_; accepted \_\_\_\_\_

---

<sup>1</sup>Department of Physics and Astronomy, Rice University, Houston, TX 77005

<sup>2</sup>Visiting Graduate Student Fellow, Spitzer Science Center, Caltech, Pasadena, CA 91125

<sup>3</sup>Spitzer Science Center, Caltech, Pasadena, CA 91125

<sup>4</sup>Max-Planck-Institüt für Astronomie, Heidelberg, Germany

<sup>5</sup>Department of Astronomy, University of Maryland, College Park, MD 20741

## ABSTRACT

We have mapped the H<sub>2</sub> S(0) – H<sub>2</sub> S(5) pure rotational lines over a strip across M51 using the *Spitzer Space Telescope* Infrared Spectrograph. We find that the molecular gas morphology of M51 varies through each line. We use the H<sub>2</sub> maps to model the H<sub>2</sub> excitation-temperature and mass across the galaxy and find that the H<sub>2</sub> exists in a continuous distribution of temperatures from 100 – 1000 K. Using the low  $J$  lines to trace the warm (T = 100 – 300 K) H<sub>2</sub>, we find that the warm H<sub>2</sub> excitation-temperature is highest in the nuclear region (192 K) and lower within the spiral arms (150 – 170 K). Using the higher  $J$  lines to trace the hot (T = 400 – 1000 K) H<sub>2</sub>, we find that the hot H<sub>2</sub> excitation-temperature is lowest in the inner spiral arms (500 – 550 K) and increases to  $\sim$  600 K in the nucleus, where the largest hot H<sub>2</sub> mass densities are found ( $0.24 \text{ M}_\odot/\text{pc}^2$ ). The warm-to-hot H<sub>2</sub> mass ratio is not constant across the galaxy indicating different primary excitation mechanisms for the warm and hot H<sub>2</sub> phases. We compare H<sub>2</sub> to CO ( $J = 1 - 0$ ) emission and find offsets between the warm and hot H<sub>2</sub> mass phases and the CO. One possible explanation for the offsets between the warm H<sub>2</sub> mass and CO is that the warm H<sub>2</sub> traces the sites of active star formation within the molecular clouds. We compare H<sub>2</sub> to H $\alpha$  emission and find the warm and hot H<sub>2</sub> mass are located in the H $\alpha$  dust lanes with the one exception being the inner spiral arms where the warm H<sub>2</sub> mass coincides with H $\alpha$  emission. In the nuclear region, the hot H<sub>2</sub> is coincident with [O IV](25.89  $\mu\text{m}$ ) emission and X-ray emission suggesting that shocks and X-rays are the dominant excitation mechanisms of the hot H<sub>2</sub> phase.

*Subject headings:* galaxies: ISM — galaxies: H<sub>2</sub> — galaxies: individual(M51)

## 1. Introduction

Star formation and galactic evolution are linked via the molecular gas within a galaxy. In the Milky Way, nearly all star formation occurs in molecular clouds (), although not all molecular clouds are actively forming stars. In galaxies star formation is triggered whenever the molecular gas surface density is enhanced, for example, by a spiral density wave (?), by increased pressure or density in galactic nuclei (??), due to the hydrodynamic shock along the leading edge of bars (??), and in the transition region at the ends of bars (?). Although the connection between star formation and molecular gas is well-established, the exact mechanisms for initiating, controlling, and inhibiting star formation are not well-understood.

M51 (the Whirlpool galaxy, NGC 5194) is a nearby, face-on spiral galaxy that is rich in molecular gas. Its proximity [assumed to be 8.2 Mpc (?)], face-on orientation, and grand-design spiral morphology make it an ideal target for studies of the ISM across distinct dynamical, chemical, and physical environments in a galaxy. Studies of the molecular gas within M51 have revealed giant molecular associations (GMAs) along the spiral arms (), a reservoir of molecular gas associated with the nuclear AGN (?), and star-formation in molecular clouds triggered by a spiral density wave (?). In addition to being well-studied at millimeter and radio wavelengths, M51 has been studied in X-rays, UV, optical, near-infrared, infrared, and submillimeter wavelengths (??; ?).

The Infrared Spectrograph (IRS) () on-board the *Spitzer Space Telescope* is a powerful tool for observing the warm ( $T = 100 - 300$  K) and hot ( $T = 400 - 1000$  K) molecular gas within galaxies. The *Spitzer* IRS low resolution modules cover 5 - 38  $\mu\text{m}$  (short-low, SL, 5 - 14  $\mu\text{m}$ ; long-low, LL, 14 - 38  $\mu\text{m}$ ) giving observers access to the lowest pure rotational H<sub>2</sub> lines with the low  $J$  lines tracing the warm molecular gas phase and the higher  $J$  lines tracing the hot molecular gas phase. These lines are important diagnostics of the ISM that

allow us to model the H<sub>2</sub> excitation-temperature, mass (?), and ortho-to-para ratio (??). By understanding the pure rotational H<sub>2</sub> line emission from a galaxy, constraints can be placed on the energy injection mechanisms (i.e. radiative heating, shocks, turbulence) that heat the warm molecular gas phase in the ISM.

In this paper we present maps of the extinction-corrected H<sub>2</sub> S(0) – H<sub>2</sub> S(5) line intensities over a strip across M51(§3.1) and use the maps to model the warm and hot H<sub>2</sub> excitation-temperature and mass across the galaxy (§3.2). We seek to understand whether the warm and hot phases undergo excitation via the same processes and discern the primary excitation mechanism of H<sub>2</sub> across the galaxy by comparing H<sub>2</sub> to CO ( $J = 1 - 0$ ), H $\alpha$ , [O IV](25.89  $\mu\text{m}$ ) intensity, and X-rays (§4).

## 2. Observations and Data Reduction

### 2.1. Spectral Data

We mapped a radial strip across M51 using the short-low (SL) and long-low (LL) modules of the *Spitzer* IRS in spectral mapping mode. The radial strips were 324''  $\times$  57'' and 295''  $\times$  51'' in the SL and LL, respectively. Integration times in the SL and LL were 14.6 s. Each slit position was mapped twice and half-slit spacings were used. In total, 1,412 spectra were taken in the SL and 100 were taken in the LL (including background observations). Dedicated off source background observations were taken for the SL observations. Backgrounds for the LL observations were taken from outrigger data collected while the spacecraft was mapping in the adjacent module. The astronomical observation requests (AORs) are available on SST's Leopard and Spot (Project ID 200138, PI: K. Sheth).

The spectra were assembled from the basic calibration data (BCD) into spectral data

cubes for each module using CUBISM (??). Background subtraction and bad pixel removal was done within CUBISM. The individual IRS spectra were processed using the S14.0 version of the Spitzer Science Center (SSC) pipeline. In CUBISM, the SL and LL data cubes have resolutions of  $1.85''/\text{pixel}$  and  $5.08''/\text{pixel}$ , respectively. The spatial resolution of the data cubes varies as a function of wavelength from  $1''85$  at  $5.2\ \mu\text{m}$  to  $13''8$  at  $38\ \mu\text{m}$ .

We created maps of the  $\text{H}_2\ \text{S}(0) - \text{H}_2\ \text{S}(5)$  lines with PAHFIT (?), a spectral fitting routine that decomposes IRS low resolution spectra. The advantage of using PAHFIT is that it allows the recovery of the full line flux of blended  $\text{H}_2$  lines such as  $\text{H}_2\ \text{S}(1)$ , blended with the  $17.0\ \mu\text{m}$  PAH complex;  $\text{H}_2\ \text{S}(2)$ , blended with  $[\text{Ne}\ \text{II}](12.8\ \mu\text{m})$ ; and  $\text{H}_2\ \text{S}(5)$ , blended into  $[\text{Ar}\ \text{II}](6.9\ \mu\text{m})$ . We ran PAHFIT through the SL (SL1 + SL2) and LL (LL1 + LL2) cubes separately. The concatenated SL and LL data cubes were each smoothed spatially by a  $3 \times 3$  pixel box prior to running PAHFIT to increase the signal-to-noise ratio of the spectra. When running PAHFIT through the SL and LL data cubes we measured the extinction-corrected line intensity of every spectral line in the data cubes while saving the information about the position (RA and Dec) of each spectrum and in doing so, we constructed line-intensity maps.

## 2.2. Ancillary Data: CO Map, $\text{H}\alpha$ Imagery, and X-ray Observations

The BIMA (Berkely Illinois Maryland Array) CO ( $J = 1 - 0$ ) map was acquired as a part of the BIMA Survey of Nearby Galaxies (SONG) (?). The beam size is  $5''.8 \times 5''.1$  ( $220\ \text{pc} \times 190\ \text{pc}$ ).

The  $\text{H}\alpha + [\text{N}\ \text{II}]$  image of M51 was observed at Kitt Peak as part of the *Spitzer Infrared Nearby Galaxies Survey* (SINGS). The pixel scale is  $0''.305$  and the flux scale is in counts/sec. Additional information about the  $\text{H}\alpha$  image can be found in the SINGS

Fourth Data Release (DR4).

X-ray emission from M51 was observed by the Advanced CCD Imaging Spectrometer (ACIS) on the *Chandra X-Ray Observatory* on 20 June 2000. The total integration time was 14,865 seconds. The resolution of the image is  $\sim 1''$ . Further details of the observations are presented in (?).

### 3. Results

#### 3.1. Morphology of H<sub>2</sub> Emission

We have detected and mapped H<sub>2</sub> emission from the six lowest pure rotational H<sub>2</sub> lines (Figure 1). The maps of H<sub>2</sub> line intensity reveal remarkable differences in the morphology of M51 through each line. H<sub>2</sub> S(0) emission is strongest in the northwest spiral arm peaking at an intensity of  $3.66 \times 10^{-18}$  W/m<sup>2</sup> and decreases by a factor of 2 in the nuclear region. The H<sub>2</sub> S(1) emission peaks in the nucleus of the galaxy at an intensity of  $1.03 \times 10^{-17}$  W/m<sup>2</sup> and shows similar intensity moving into the northwest spiral arm. The peaks in H<sub>2</sub> S(0) and H<sub>2</sub> S(1) emission within the arms are not aligned, they are offset by 10''.2 (380 pc). These offsets are not a result of the difference in resolution between the two maps, but appear to be real. H<sub>2</sub> S(0) and H<sub>2</sub> S(1) emission is resolved out to 5 – 6 kpc from the nucleus of the galaxy in the northwest outer spiral arm. In the outer spiral arm, the H<sub>2</sub> S(0) intensity is a factor of 2 times lower than in the inner northwest spiral arm and the H<sub>2</sub> S(1) intensity is a factor of 5 times lower than in the nucleus of M51.

The H<sub>2</sub> S(2) – H<sub>2</sub> S(5) maps show different molecular gas morphology within M51 through each H<sub>2</sub> line. The strongest H<sub>2</sub> S(2) emission is from the nuclear region peaking at  $2.21 \times 10^{-18}$  W/m<sup>2</sup>. We also see bright H<sub>2</sub> S(2) emission from the inner northwest spiral arm; however, the intensity is a factor of 2 lower than in the nucleus. The H<sub>2</sub> S(3) line

exhibits similar strong emission in the nuclear region. The H<sub>2</sub> S(3) intensity in the nucleus is  $1.35 \times 10^{-17}$  W/m<sup>2</sup> which is a factor of  $\sim 6$  greater than the intensity of H<sub>2</sub> S(2) nuclear emission. We see an apparent bar structure in H<sub>2</sub> S(3) emission across the nucleus of the galaxy going north-to-south. We see offsets in the intensity peaks within the spiral arms between the H<sub>2</sub> S(2) and H<sub>2</sub> S(3) maps. An example of this is in the northwest inner spiral arm. In H<sub>2</sub> S(2) emission, we see bright ( $1.30 \times 10^{-18}$  W/m<sup>2</sup>) H<sub>2</sub> emission to the north of the nucleus. The H<sub>2</sub> S(2) intensity decreases to  $7.00 \times 10^{-19}$  W/m<sup>2</sup> moving southwest in the spiral arm. In the H<sub>2</sub> S(3) emission map, we see the H<sub>2</sub> S(3) intensity increasing from  $4.00 \times 10^{-18}$  W/m<sup>2</sup> to  $5.10 \times 10^{-18}$  W/m<sup>2</sup> as we move from north of the nucleus (the end of the bar structure) to the southwest in the inner spiral arm. The offsets in the peak emission of the H<sub>2</sub> lines are real and indicate variations in the excitation-temperature in each region.

The H<sub>2</sub> S(4) and H<sub>2</sub> S(5) lines are faint across the disk of the galaxy but both are very strong in the nuclear region. In the nucleus, the H<sub>2</sub> S(4) intensity is  $3.05 \times 10^{-18}$  W/m<sup>2</sup> and the H<sub>2</sub> S(5) intensity is  $8.04 \times 10^{-18}$  W/m<sup>2</sup>. H<sub>2</sub> S(5) emission is asymmetric in the nucleus and mimics the morphology of the H<sub>2</sub> S(3) line with extended emission to the north of the nucleus. The H<sub>2</sub> S(4) line shows emission in the nucleus and in the spiral arm to the west. In the spiral arm to the west of the nucleus, the H<sub>2</sub> S(4) intensity is  $2.11 \times 10^{-18}$  W/m<sup>2</sup>. This is notable because the spiral arm to the southwest of the nucleus is very bright in CO and studies have revealed very high molecular gas column densities in the southwest inner spiral arm ( ). The differences in the morphology of H<sub>2</sub> emission are indicative of changes in the H<sub>2</sub> excitation-temperature across the galaxy, which we discuss in the next section.

### 3.1.1. Note on Uncertainties in the H<sub>2</sub> Line Intensity Maps

The uncertainty in the H<sub>2</sub> line intensity varies as a function of line intensity across each map. The uncertainty in the H<sub>2</sub> S(0) line intensity ranges from 20 – 40 % across the nuclear region and spiral arms. The uncertainty in the spiral arm intensity at greater distances from the center of the strip is 80 – 90 %. The H<sub>2</sub> S(1) line map has lower uncertainties with the uncertainty being ∼ 10 % in the nuclear region and 20 – 30 % in the spiral arms. The H<sub>2</sub> S(2) and H<sub>2</sub> S(3) lines show similar uncertainties to each other. In the nuclear region their uncertainty is 10 – 30 % and in the spiral arms their uncertainty is 50 – 80 %. The H<sub>2</sub> S(4) and H<sub>2</sub> S(5) lines only show emission from the nuclear region; their uncertainties in the line intensity are ∼ 35 % and 25 %, respectively.

## 3.2. Mapping H<sub>2</sub> Excitation-Temperature and Mass across M51

### 3.2.1. Modeling H<sub>2</sub> Excitation-Temperature and Mass

The pure rotational lines of molecular hydrogen provide a powerful probe of the conditions of the ISM and place constraints on the energy injection processes that excite H<sub>2</sub> (?). From the maps of H<sub>2</sub> S(0) – H<sub>2</sub> S(5) emission, we have modeled the H<sub>2</sub> excitation-temperature and mass (?) across M51.

In order to model the H<sub>2</sub> excitation and mass across the galaxy, the H<sub>2</sub> S(1) – H<sub>2</sub> S(5) maps were smoothed to the resolution of the H<sub>2</sub> S(0) map. The maps were then interpolated to the same spatial grid. Excitation diagrams across the strip were derived from the Boltzman equation using the formulation from Rigopoulou et al. (2002),

$$N_i/N = (g(i)/Z(T_{\text{ex}})) \exp(-T_i/T_{\text{ex}}) \quad (1)$$

where  $g(i)$  is the statistical weight of state  $i$ ,  $Z(T_{\text{ex}})$  is the partition function,  $T_i$  is the

energy level of a given state, and  $T_{\text{ex}}$  is the excitation temperature.  $N$  and  $N_i$  are the total column density and the column density of a given state  $i$  and  $N_i$  is determined directly from the measured extinction-corrected flux by

$$N_i = 4\pi \times \text{flux}(i) / (\Omega A(i) h \nu(i)) \quad (2)$$

where  $A(i)$  is the  $A$ -coefficient,  $\nu(i)$  is the frequency of state  $i$ ,  $\Omega$  is the solid angle of the beam, and  $h$  is Planck's constant. Table 1 lists the values for the wavelength, rotational state, Einstein  $A$ -coefficient, energy, and statistical weight of the pure rotational levels of  $H_2$  that we have observed with the *Spitzer* IRS.

In Figure 2 we present excitation diagrams from three different regions across the M51 strip. The excitation diagrams exhibit an ortho-to-para ratio (OPR) of 3 in the nuclear region. This is in agreement with the value of the OPR of the nuclear region determined by SINGS (?). Outside the nucleus, the lower  $J$  ( $H_2$  S(0) -  $H_2$  S(3)) levels exhibit an OPR of 3. The  $H_2$  S(4) measurement shows significant scatter in the excitation diagrams outside of the nuclear region of M51. This would indicate that the OPR is less than 3; however, due to the low signal-to-noise ratio of the  $H_2$  S(4) map, we do not believe that the OPR determined from the  $H_2$  S(4) intensity reflects the OPR of the warm  $H_2$ . The excitation-diagrams also exhibit a change in slope as a function of rotational level. This indicates that a continuous distribution of  $H_2$  temperatures is being sampled within the beam.

Because the excitation diagrams shown in Figure 2 indicate that we are sampling a range of excitation-temperatures in different regions across the M51 strip, we assume that the  $H_2$  exists in the form of two discrete components. We define these two components as a warm ( $T = 100 - 300$  K)  $H_2$  phase and a hot ( $T = 400 - 1000$  K)  $H_2$  phase. We determine the excitation-temperature and mass distribution of the hot ( $T = 400 - 1000$  K)  $H_2$  phase from the least squares fit to the  $H_2$  S(2) -  $H_2$  S(5) lines in the excitation diagram. We determine the excitation-temperature and mass distribution of the warm ( $T = 100 -$

300 K) H<sub>2</sub> phase from the least squares fit to the H<sub>2</sub> S(0) – H<sub>2</sub> S(2) lines in the excitation diagram; however, because the warm and hot H<sub>2</sub> phases are inherently coupled, we subtract the contribution of the hot H<sub>2</sub> from the warm H<sub>2</sub> in order to determine the warm H<sub>2</sub> excitation-temperature and mass (Higdon et al. 2006).

### 3.2.2. Warm and Hot H<sub>2</sub> Mass Distributions

In Figure 3 we present the warm (*left*) and hot (*right*) H<sub>2</sub> mass distributions across the M51 strip. Note that the non-rectangular shape of the strip is due to the offset between the SL and LL strips. Also note that the sizes of the plots of the warm and hot H<sub>2</sub> mass phases are different. The warm H<sub>2</sub> mass is determined from the H<sub>2</sub> S(0) – H<sub>2</sub> S(2) maps of the H<sub>2</sub> emission across the entire strip. The hot H<sub>2</sub> mass is determined from the higher *J* rotational states for which the H<sub>2</sub> emission is not well-resolved across the strip. The warm H<sub>2</sub> mass peaks in the inner northwest spiral arm with 11 M<sub>⊙</sub>/pc<sup>2</sup> warm H<sub>2</sub>. The mass in the outer northwest and southeast spiral arms peaks toward the center of the spiral arms with 3.5 M<sub>⊙</sub>/pc<sup>2</sup> warm H<sub>2</sub> and 1.0 M<sub>⊙</sub>/pc<sup>2</sup> warm H<sub>2</sub> (in the northwest and southeast arms, respectively).

The peak in hot H<sub>2</sub> mass appears to be bimodal with a peak in the nucleus of the galaxy containing 0.24 M<sub>⊙</sub>/pc<sup>2</sup> and a second peak that is interior to the inner spiral arm, also containing 0.24 M<sub>⊙</sub>/pc<sup>2</sup>. The hot H<sub>2</sub> mass in the spiral arms is only ∼ 20 - 30 % of the hot H<sub>2</sub> mass in the nucleus. We would like to note that in M51, we are sensitive to 0.40 M<sub>⊙</sub>/pc<sup>2</sup> warm H<sub>2</sub> and 0.005 M<sub>⊙</sub>/pc<sup>2</sup> hot H<sub>2</sub> within our beam.

### 3.2.3. Warm and Hot H<sub>2</sub> Excitation-Temperature Distributions

In Figure 4 we compare the warm H<sub>2</sub> mass distribution to the excitation-temperature. The gas is warmest in the nuclear region of M51 with the temperature ranging from 175 – 190 K in the center of the galaxy. The gas is cooler within the spiral arms of M51 than in the inter-arm regions. The temperature in this spiral arm decreases from 175 K at the outer surface layers to 154 K in the most dense region of the arm indicating that the warm H<sub>2</sub> excitation-temperature is cooler at higher H<sub>2</sub> densities. In the outer northwest and southeast spiral arms (at 5 – 6 kpc from the center of the galaxy each) molecular the gas excitation-temperature ranges from 150 K at the center to about 175 K near the edge of the spiral arms; again indicating that high density regions are cooler than low density regions.

The excitation-temperature distribution of the hot H<sub>2</sub> is shown in Figure 5 and reveals a different picture than the excitation-temperature distribution of the warm H<sub>2</sub>. The excitation-temperature in the nuclear region ranges from 587 to 612 K. The excitation-temperature in the northwest inner spiral arm is the coolest at 538 K. The hottest excitation-temperatures are observed in the inter-arm regions where there is the least amount of H<sub>2</sub>. In contrast, in the southeast inter-arm region, the excitation temperature is in excess of 900 K.

## 4. Discussion

### 4.1. Comparison to Previous Studies of Warm and Hot H<sub>2</sub> in Galaxies

Previous studies of pure rotational H<sub>2</sub> emission in galaxies have used aperture average spectra over the central regions of galaxies to derive the excitation temperature and mass of the warm and hot molecular gas phases within a galaxy (?; ?). SINGS has studied molecular hydrogen in M51 and finds that within the central 330 arcsec<sup>2</sup>, the excitation-temperature

and mass of the warm ( $T = 100 - 300$  K)  $H_2$  phase are  $T = 180$  K and  $M_{\text{warm}} = 1.46 \times 10^6 M_\odot$ , respectively (?). Within the central  $412 \text{ arcsec}^2$  of M51, we measure a warm  $H_2$  excitation-temperature of  $186$  K and mass of  $1.63 \times 10^6 M_\odot$ , consistant with the SINGS to within 10 %. SINGS also measures the excitation-temperature of the hot phase (though they do not measure the mass in the hot phase) and find a hot  $H_2$  excitation-temperature of  $521$  K. Over the nuclear region of M51, we measure an excitation-temperature of  $584$  K.

Rigopoulou et al. (2002) measured the  $H_2$  mass in the hot phase and found that the warm-to-hot mass fraction varies between  $5 \times 10^3 - 1 \times 10^6$  for Seyferts. This is significantly higher than the warm-to-hot mass fraction (Figure 6) than we measure within the central  $412 \text{ arcsec}^2$  of M51,  $14.8$ . To measure the hot  $H_2$  mass, we use the  $H_2 S(2) - H_2 S(5)$  lines, whereas Rigopoulou et al. (2002) used the  $H_2 S(5) - H_2 S(7)$  lines. Thus, the hot  $H_2$  phase that they measured is preferentially offset to higher  $H_2$  excitation-temperatures and lower  $H_2$  masses.

#### 4.2. The Warm-to-Hot $H_2$ Mass Ratio

In Figure 6, we compare the warm  $H_2$  mass distribution to the hot  $H_2$  mass distribution. The warm  $H_2$  mass distribution peaks at in the northwest inner spiral arm and the hot  $H_2$  mass distribution peaks at in the nucleus and in the region interior to the northwest spiral arm. It is evident from the figure that the warm-to-hot  $H_2$  mass ratio is not constant across the galaxy but is lowest in the nucleus of the galaxy (at 12) and increases to 170 and 136 in the southeast and northwest spiral arms, respectively. The differences between the warm and hot  $H_2$  mass distributions and the variations in the morphology of M51 as a function of rotational energy level suggest different origins to the warm and hot  $H_2$  phases and that the primary excitation mechanisms of the warm and hot  $H_2$  phases differ.

In order to understand the H<sub>2</sub> excitation and where each excitation mechanism is dominant, we made comparisons of the H<sub>2</sub> line intensity and mass distributions to diagnostics of three excitation mechanisms: UV photons emitted in dense photon dominated regions (PDRs) and H II regions, shocks, and X-rays. We use CO ( $J = 1 - 0$ ) emission to determine the location of the H<sub>2</sub> relative to locations dense PDRs, H $\alpha$  imagery to identify H II regions (?), [O IV](25.98  $\mu\text{m}$ ) line emission as a diagnostic of shocks (?), and the 0.5 – 10.0 keV X-ray band to distinguish X-ray dominated regions (XDRs). The following section compares the H<sub>2</sub> mass distributions to CO ( $J = 1 - 0$ ), H $\alpha$ , [O IV], and X-ray emission.

### 4.3. Distinguishing the H<sub>2</sub> Excitation Mechanisms

#### 4.3.1. H<sub>2</sub> Excitation by UV Photons from PDRs: Comparison of H<sub>2</sub> to CO Emission

In star-forming regions, H<sub>2</sub> exists within the PDR and deep into the molecular cloud. Owing to a low dissociation energy of 4.5 eV, H<sub>2</sub> formation generally does not occur within a PDR until the radiation field becomes sufficiently weak. Understanding H<sub>2</sub> in PDRs and implementing H<sub>2</sub> into photoionization codes has become the emphasis of many theoretical models. Recent advances in the CLOUDY photoionization code have included H<sub>2</sub> and modeled the structure of star-forming regions while treating the H II region and PDR as one continuous cloud (?). Kaufman et al. (2006) used Starburst99/Mappings to model H<sub>2</sub> pure rotational line emission from PDRs to probe the conditions of dense PDRs in star-forming regions. They show that within galaxies, where the telescope beam size is generally kiloparsecs across, H<sub>2</sub> emission could serve to probe the surface layers of dense molecular clouds.

CO is found deep within a molecular cloud where the temperatures are too cold to excite H<sub>2</sub> emission. In these regions, CO is collisionally excited by the more abundant H<sub>2</sub>

molecule. CO is connected to H<sub>2</sub> in star-forming regions because at the surface layers of the molecular clouds, H<sub>2</sub> is excited and CO emits dipole rotational lines due to heating by the ionizing radiation of newborn massive stars () .

In Figure 7, we compare the warm (*left*) and hot H<sub>2</sub> (*right*) mass distributions to CO (J = 1 – 0) emission. The brightest CO emission is seen in the spiral arms where the greatest amounts of warm H<sub>2</sub> mass are also found. The most striking result is that in the inner spiral arms, we see that the CO is offset toward the nucleus from the warm H<sub>2</sub> mass. The offset between the peaks in CO and warm H<sub>2</sub> mass is 7''.2 in the northwest spiral arms and 5'' in the southeast spiral arms. We believe that these offsets are real with one possible explanation being that the H<sub>2</sub> is tracing the regions of active star-formation within the giant molecular associations.

We compare CO to the hot H<sub>2</sub> mass distribution (Figure 7, *right*) and we see that the hot H<sub>2</sub> mass is most abundant in the nuclear region, interior to the CO bright spiral arms. In northwest spiral arm, the hot H<sub>2</sub> mass is offset from the CO by 2''.6. We believe that the offsets between the CO and the hot H<sub>2</sub> mass are real, however, they are likely due to the dominance of other excitation mechanisms (shocks or X-rays) in the nuclear region of M51.

In Figure 8, we compare the CO intensity to the H<sub>2</sub> S(0) – H<sub>2</sub> S(3) line intensity maps. We see that the H<sub>2</sub> S(0) contours trace the CO spiral arms with one notable difference being that we detect H<sub>2</sub> S(0) emission far (5 – 6 kpc) from the nucleus of M51, where there is no CO detected. The H<sub>2</sub> S(1) – H<sub>2</sub> S(3) contours also trace the CO spiral arms; however, within the spiral arms, the H<sub>2</sub> is not necessarily aligned with the CO. For example, in the comparison of H<sub>2</sub> S(3) to CO, we see that in the inner spiral arms, the H<sub>2</sub> contours trace the CO; however, within the northwest arm, we see that there is strong H<sub>2</sub> emission offset to the west by 9''.3 from the bright CO emission in the same spiral arm. The offsets between the peaks in H<sub>2</sub> and CO emission are not systematic in any direction.

The CO intensity in the nucleus of the galaxy is much fainter than in the bright CO spiral arms. This is interesting because  $\text{H}_2 \text{ S}(1) - \text{H}_2 \text{ S}(3)$  emission is brightest in the nucleus of M51 where  $\text{H}_2$  emission from the higher  $J$  lines is likely due to more energetic processes such as shock excitation and X-rays (which we discuss in §4.3.3 and §4.3.4).

#### 4.3.2. $\text{H}_2$ Excitation by UV Photons from H II Regions: Comparison of $\text{H}_2$ to $\text{H}\alpha$ Emission

H II regions are sites of recent massive star formation. They illuminate bright nebulae in distant galaxies and outline the spiral arms. H II regions emit prodigious amounts of UV radiation at energies  $\geq 13.6$  eV capable of exciting and ionizing  $\text{H}_2$ .  $\text{H}\alpha$  imagery is often used to identify and map H II regions in star-forming galaxies. Scoville et al. (2001) used  $\text{H}\alpha$  and  $\text{Pa}\alpha$  imagery to identify and characterize over 1,350 H II regions in M51.

In Figure 9, we compare the warm (*left*) and hot (*right*)  $\text{H}_2$  mass distributions to  $\text{H}\alpha$  emission. In general, the warm and hot  $\text{H}_2$  concentrations are not cospatial with the  $\text{H}\alpha$  emission regions in the spiral arms with the one exception being that the warm  $\text{H}_2$  mass in the inner spiral arms appears to trace the  $\text{H}\alpha$  emission. The warm  $\text{H}_2$  mass contours show that local peaks in  $\text{H}_2$  mass are found within the dust lanes. An example of this is in the northwest spiral arms where we see the  $\text{H}_2$  mass offset from the  $\text{H}\alpha$  spiral arms with local peaks being found in the dust lanes.

In Figure 10, we compare the  $\text{H}_2 \text{ S}(0) - \text{H}_2 \text{ S}(3)$  line intensity maps to  $\text{H}\alpha$  emission. Comparison of the  $\text{H}_2 \text{ S}(0)$  map to  $\text{H}\alpha$  reveals that the strongest  $\text{H}_2$  emission in the northwest and southeast inner spiral arms is coincident with  $\text{H}\alpha$  emission; however, the other  $\text{H}_2 \text{ S}(0)$  spiral arms show the strongest emission in the dust lanes, offset from the  $\text{H}\alpha$  spiral arms. The largest offsets are seen in the southwest spiral arm where the  $\text{H}_2 \text{ S}(0)$

emission is offset from the H $\alpha$  spiral arm by  $\sim 15''$  (560 pc). H<sub>2</sub> S(1) emission appears to follow the dust lanes and the H<sub>2</sub> S(1) intensity subsides into the H $\alpha$  spiral arms. H<sub>2</sub> S(2) and H<sub>2</sub> S(3) emission is also found in the dust lanes; however, there are instances (such as in the southeast spiral arm) where the H<sub>2</sub> emission appear to be found straddling the dust lane and H $\alpha$  spiral arm.

These results are in contradiction to a previous study of rovibrational H<sub>2</sub> line emission in Seyfert galaxies by Quillen et al. (1999) who used *HST* NICMOS to map the H<sub>2</sub>(1-0)S(1) (2.121  $\mu\text{m}$ ) and H<sub>2</sub>(1-0)S(3)(1.957  $\mu\text{m}$ ) lines in 10 Seyfert galaxies. They found that the H<sub>2</sub> emission is generally coincident with H $\alpha$  emission and near the dust lanes (though offset from them). One explanation for this could be that the rovibrational lines trace a much hotter (1000 – 5000 K) molecular gas which can be found associated with H II regions whereas the cooler H<sub>2</sub> traced by the lowest pure rotational transitions is found in dense PDRs and molecular clouds associated with star forming regions.

#### 4.3.3. H<sub>2</sub> Excitation by Shocks: Comparison of H<sub>2</sub> to [O IV](25.89 $\mu\text{m}$ ) Emission

The [O IV](25.89  $\mu\text{m}$ ) line can be excited in shocks (?), the stellar winds of massive Wolf-Rayet stars (?), or by an active galactic nucleus (AGN)(?). Though the [O IV] line is blemmed with the [Fe II](25.99  $\mu\text{m}$ ) line in *Spitzer* IRS low resolution spectra, PAHFIT can deblend the two lines and in mapping the H<sub>2</sub> S(0) and H<sub>2</sub> S(1) line in the LL data cubes, we also mapped the [O IV] line.

In Figure 11, we compare the [O IV] intensity to the warm (*left*) and hot (*right*) H<sub>2</sub> distributions. The [O IV] emission is brightest in the nuclear region at  $8.75 \times 10^{-18} \text{ W/m}^2$  and the peak is coincident with the nuclear peak in the mass of the hot H<sub>2</sub>. [O IV] emission subsides from the nucleus to the inner spiral arm by 50 %. We resolve weaker [O IV]

emission within the warm and hot H<sub>2</sub> spiral arms. The [O IV] intensity in the spiral arms is a factor of  $\sim 6$  lower in the spiral arms than the peak intensity found in the nucleus.

The [O IV] emission within the nuclear region of M51 is likely due to the weak Seyfert II nucleus () and is possibly associated with shocked gas from the outflows of the AGN. The peak of the [O IV] emission coincides with the nuclear peak in hot H<sub>2</sub> mass indicating that the hot H<sub>2</sub> phase in the nuclear region of the galaxy is AGN or shock heated. With  $2.43 \times 10^5 M_{\odot}$  of hot H<sub>2</sub> in the central 0.58 kpc<sup>2</sup>, it is unlikely that the hot H<sub>2</sub> is fueling the central AGN, but is excited by the AGN or shocks produced by it. In the nuclear region we observe a factor of 12 times greater warm H<sub>2</sub> mass. The warm H<sub>2</sub> mass is much greater within the spiral arms than within the nucleus and the warm-to-hot mass ratio is lowest in the nuclear region where the [O IV] intensity is greatest. In the nuclear region, shocks appear to be a more efficient means to excite the hot H<sub>2</sub> phase than the warm H<sub>2</sub> phase.

#### 4.3.4. H<sub>2</sub> Excitation by X-rays: Comparison of H<sub>2</sub> to X-ray Emission

M51 has been extensively studied in X-rays by ASCA (?), Newton XMM (), and the Chandra X-ray Observatory (?). These observations of M51 have revealed more than 80 X-ray sources. Candidates for these X-ray sources include neutron stars, black holes, supernova remnants (SN 1994I), and a low-luminosity AGN (; ?). X-ray emission from the nuclear region of M51 has been studied by Terashima and Wilson (2001). They observe X-ray emission from the nucleus, the extranuclear cloud (XNC, to the south of the nucleus), and the northern loop. A radio jet has been observed connecting the nucleus of M51 to the XNC in 6 cm imagery (). The jet emanates from the south of the elongated nucleus and is shock heating ISM.

In Figure 12, we compare the smoothed 0.5 - 10 keV band X-ray image to the warm

(*left*) and hot (*right*) H<sub>2</sub> mass distributions. The 0.5 - 10 keV band has been smoothed to the resolution of the warm and hot H<sub>2</sub> mass distributions and the nucleus, XNC, and northern loop are indistinguishable in the smoothed image. X-ray emission is most intense from the nucleus and decreases into the northwest spiral arm that contains the greatest H<sub>2</sub> mass. There appears to be very little connection between the 0.5 - 10 keV X-ray band and the warm H<sub>2</sub> mass distribution.

The peak in X-ray emission is coincident with the hot H<sub>2</sub> mass peak. The most intense 0.5 - 10 keV X-ray emission originates from the nucleus and is oriented north-to-south, similar to the [O IV](25.89  $\mu$ m) emission. The peak in X-ray emission is located within the peak in hot H<sub>2</sub> mass suggesting that X-rays play an important role in exciting the hot H<sub>2</sub> phase. While there is a correlation between X-ray emission and the hot H<sub>2</sub> phase, H<sub>2</sub> excitation by X-rays cannot be distinguished from H<sub>2</sub> excitation by shocks.

We further investigate X-ray excited H<sub>2</sub> emission in M51 by comparing the 0.5 – 10.0 keV X-ray band to the H<sub>2</sub> S(2) – H<sub>2</sub> S(5) line intensity maps (Figure 13). The H<sub>2</sub> S(2) – H<sub>2</sub> S(5) line intensities all peak at the X-ray source within the nucleus. The X-ray source fits within the H<sub>2</sub> contours because the X-ray image resolution is slightly higher than the resolution of each of the H<sub>2</sub> maps.

The morphology of the nuclear H<sub>2</sub> emission appears to be correlated with the X-ray source. The H<sub>2</sub> S(2) intensity peaks around the X-ray nucleus and the intensity decreases to the south by 70 % in the southern XNC. The bar structure seen in the H<sub>2</sub> S(3) emission is aligned with X-ray emission from the nucleus, XNC, and northern loop. The H<sub>2</sub> S(3) intensity peaks between the X-ray nucleus and the XNC. To the north of the nucleus, the contours follow the X-ray loop. To the south of the nucleus (into the XNC), H<sub>2</sub> S(3) intensity decreases by 80 %. The H<sub>2</sub> S(4) and H<sub>2</sub> S(5) line intensities are highest in the nucleus which coincides with strong X-ray emission from the nucleus and XNC.

## 5. Conclusions

We have spectrally mapped a strip across M51 using the *Spitzer* IRS low resolution modules. We used the spatially resolved spectra to map H<sub>2</sub> S(0) – H<sub>2</sub> S(5) line intensities across the strip. We find:

1. The morphology of H<sub>2</sub> emission in M51 varies with H<sub>2</sub> rotational level. H<sub>2</sub> S(0) emission is strongest in the spiral arms of the galaxy while the higher  $J$  transitions show the strongest emission towards the nucleus. The H<sub>2</sub> S(1) intensity is strongest in the nuclear region and in the northwest spiral arms, however, the peak in H<sub>2</sub> S(0) intensity in the northwest spiral arm is offset from the peak in H<sub>2</sub> S(0) intensity by 10''.2. The H<sub>2</sub> S(2) and H<sub>2</sub> S(3) maps show H<sub>2</sub> emission in the nucleus, spiral arms, and inter-arm regions of M51 and bar structure aligned north-to-south is apparent in H<sub>2</sub> S(3) emission. H<sub>2</sub> S(4) and H<sub>2</sub> S(5) emission is resolved in the nuclear region of M51.
2. The different morphologies of H<sub>2</sub> emission in M51 indicate significant spatial variations in H<sub>2</sub> excitation-temperature and mass. Excitation diagrams reveal that the H<sub>2</sub> exists in a continuous distribution of temperatures across the galaxy. Using the low  $J$  lines to trace the warm (T = 100 – 300 K) H<sub>2</sub>, we find that the warm H<sub>2</sub> excitation-temperature is highest in the nuclear region at 192 K and the warm H<sub>2</sub> mass peaks in the northwest inner spiral arm at a mass density of 11 M<sub>⊙</sub>/pc<sup>2</sup>. Using the higher  $J$  lines to trace the hot (T = 400 – 1000 K) H<sub>2</sub>, we find that the hot H<sub>2</sub> excitation-temperature is lowest in the inner spiral arms (500 – 550 K) and increases to ∼ 600 K in the nucleus, where the largest hot H<sub>2</sub> mass densities are found to be 0.24 M<sub>⊙</sub>/pc<sup>2</sup>.
3. The warm and the hot H<sub>2</sub> mass distributions are not cospatial and the warm-to-hot mass ratio varies across M51. The hot mass distribution shows two peaks, one in the

nucleus of M51 and one located interior to the northwest inner spiral arm of M51. The warm mass distribution peaks in the northwest spiral arm and is offset from the hot mass peak by  $11''.4$ . The warm-to-hot mass ratio varies across the galaxy with the ratio being  $\sim 15$  in the nucleus and increasing to  $> 100$  in the spiral arms. Variations in the warm-to-hot H<sub>2</sub> mass ratio and differences in the morphology of the H<sub>2</sub> emission across M51 indicate that the primary excitation mechanism differs for the warm and hot H<sub>2</sub> mass phases as a function of location within the galaxy.

4. CO emission is offset from the warm H<sub>2</sub> mass in the inner spiral arms of M51. These apparent offsets are real and are possibly associated with the regions of active star formation within the molecular clouds. In the spiral arms, the H<sub>2</sub> S(0) – H<sub>2</sub> S(3) contours trace the CO; however, within the spiral arms, the peaks in H<sub>2</sub> can be offset from the peaks in CO intensity. In the nucleus, the H<sub>2</sub> S(1) – H<sub>2</sub> S(3) lines are brightest and the CO intensity is a factor of  $\sim 2.5$  weaker than in the spiral arms suggesting that H<sub>2</sub> emission from the higher  $J$  lines is excited by shocks of X-rays.
5. Comparing the distributions of H<sub>2</sub> to H $\alpha$  reveals that the warm and hot H<sub>2</sub> mass is found in the dust lanes rather than at or around the H $\alpha$  emission regions with the one exception being that the warm H<sub>2</sub> mass in the inner spiral arms is coincident with bright H $\alpha$  emission. This is in contradiction to previous studies of spatially resolved rovibrational H<sub>2</sub> line emission in Seyferts that found the H<sub>2</sub> emission to be coincident with the H $\alpha$  emission.
6. The peaks in [O IV](25.89  $\mu\text{m}$ ) intensity and and X-ray intensity are both coincident with the peak in hot H<sub>2</sub> mass in the nucleus of M51 suggesting that the hot H<sub>2</sub> in the nucleus is primarily excited by the AGN, shocks (possibly associated with the AGN), or X-rays associated with the AGN. The spatial distributions of the [O IV] emission and X-ray

surface brightness are very similar, but a primary excitation mechanism (shocks or X-rays) of the hot H<sub>2</sub> mass phase cannot be distinguished. Further comparison of the H<sub>2</sub> S(2) – H<sub>2</sub> S(5) intensity maps to the X-ray surface brightness reveal that the nuclear H<sub>2</sub> emission is associated with X-rays and the bar structure apparent in the H<sub>2</sub> S(3) map is aligned with the nucleus, XNC, and northern loop.

The author graciously acknowledges the Spitzer Science Center Spitzer Visiting Graduate Student Fellowship program and committee for providing support for this research. The author would like to specifically acknowledge the program coordinators, Phil Appleton and Alberto Noriega-Crepso. The author would also like to thank JD Smith for swift responses to questions about PAHFIT and CUBISM and Nicolas Flagey for productive discussions about PAHFIT. Partial support for the completion and preparation for publication of this study by the author was provided by AURA grant GO10822.1 to RIce University.

*Facilities:* Spitzer Science Center (SSC), Spitzer Space Telescope (SST), Berkely-Illinois-Maryland Array (BIMA).

## REFERENCES

- Aalto, S., Hüttemeister, S., Scoville, N.Z., and Thaddeus, P., 1999, AJ, 522, 165
- Abel, N.P., Ferland, G.J., Shaw, G., and van Hoof, P.A.M., 2005, ApJS, 161, 65
- Allen, R.J., Heaton, H.I., and Kaufman M.J., 2004, ApJ, 608, 314
- Blitz, L., 1995, SSR, 684
- Calzetti, D. et al., 2005, ApJ, 633, 871
- Carpenter, J.M. and Sanders, D.B., 1998, AJ, 116, 1856
- Crane, P.C. and van der Hulst, J.M., 1992, AJ, 103, 1146
- Dewangan, G.C., Griffiths, R.E., Choudhury, M., Miyaji, T., and Schurch, N.J., 2005, ApJ, 635, 198
- Ford, H.C., Crane, P.C., Jacoby, G.H., Lawrie, D.G., and van der Hulst, J.M., 1985, ApJ, 293, 132
- Helfer, T.T., Thornley, M.D., Regan, M.W., Wong, T., Sheth, K., Vogel, S.N., Blitz, L., and Bock, D.C.J., 2003, ApJS, 145, 259
- Higdon, S.J.U., Armus, L., Higdon, J.L., Soifer, B.T., and Spoon, H.W.W., 2006, ApJ, 648, 323
- Houck, J.R. et al., 2004, ApJS, 145, 18
- Immler, S., Wilson, A.S., and Terashima, Y., 2002, ApJ, 573, L27
- Kaufman, M.J., Wolfire, M.G., and Hollenbach, D.J., 2006, ApJ, 644, 283
- Lord, S.D. and Young, J.S., 1990, ApJ, 356, 135

- Lutz, D., Kunze, D., Spoon, H.W.W., and Thornley, M.D., 1998, A&A, 333, L75
- Kennicutt, R.C. et al., 2003, PASP, 115, 928
- Kenny, J.D.P. and Lord, S.D., 1991, ApJ, 381, 118
- Matsushita, S. et al., 2004, ApJ, 616, L55
- Neufeld, D.A., Melnick, G.J., and Harwit, M., 1998, ApJ, 506, L75
- Neufeld, D.A., Melnick, G.J., Sonnentrucker, P., Bergin, E.A., Green, J.D., Kim, K.H., Watson, D.M., Forrest, W.J., and Pipher, J.L., 2006, ApJ, 649, 816
- Palumbo, G.G.C., Fabbiano, G., Fransson, C., and Trinchieri, G., 1985, ApJ, 298, 259
- Quillen, A.C., Alonso-Herrero, A., Rieke, M.J., Rieke, G.H., Ruiz, M., Kulkarni, V., 1999, ApJ, 527, 696
- Regan, M.W., Thornley, M.D., Helfer, T.T., Sheth, K., Wong, T., Vogel, S.N., Blitz, L., and Bock, D.C.J., 2001, ApJ, 561, 218
- Rigopoulou, D., Kunze, D., Lutz, D., Genzel, R., and Moorwood, A.F.M., 2002, A&A, 389, 374
- Roussel, H. et al., 2007, in press
- Schaerer, D. and Stasinska, G., 1999, A&A, 345, L17
- Scoville, N.Z. and Young, J.S., 1983, AJ, 265, 148
- Scoville, N.Z., Yun, M.S., Armus, L., and Ford, H., 1998, ApJ, 493, L63
- Scoville, N.Z., Polletta, M., Ewald, S., Stolovy, S.R., Thompson, R., and Rieke, M., 2001, AJ, 122, 3017

Shaw, G., Ferland, G.J., Abel, N.P., Stancil, P.C., and van Hoof, P.A.M., 2005, ApJ, 624, 794

Sheth, K., Regan, M.W., Vogel, S.N., and Teuben, P.J., 2000, ApJ, 532, 221

Sheth, K., Vogel, S.N., Regan, M.W., Tueben, P.J., Harris, A.I., and Thornley, M.D., 2002, AJ, 124, 2581

Sheth, K., Vogel, S.N., Regan, M.W., Thornley, M.D., and Teuben, P.J., 2005, ApJ, 632, 217

SINGS: The Spitzer Infrared Nearby Galaxies Fouth Data Delivery, May 2006.

Smith, J.D.T. et al., 2004, ApJS, 154, 199

Smith, J.D.T. et al., 2007, ApJ, 656, 770

Terashima, Y., Ptak, A., Fujimoto, M.I., Kunieda, H., Makishima, K., and Sherlemitsos, P.J., 1998, ApJ, 496, 210

Terashima, Y. and Wilson, A.S., 2001, ApJ, 560, 139

Tully, R.B. 1988, Nearby Galaxies catalog (Cambridge:Cambridge University Press)

Vogel, S.N., Kulkarni, S.R., and Scoville, S.Z., 1988, Nature, 334, 402

Young, J.S. and Devereux, N.A., 1991, ApJ, 373, 414

Young, J.S. and Scoville, N.Z., 1991, ARA&A, 29, 581

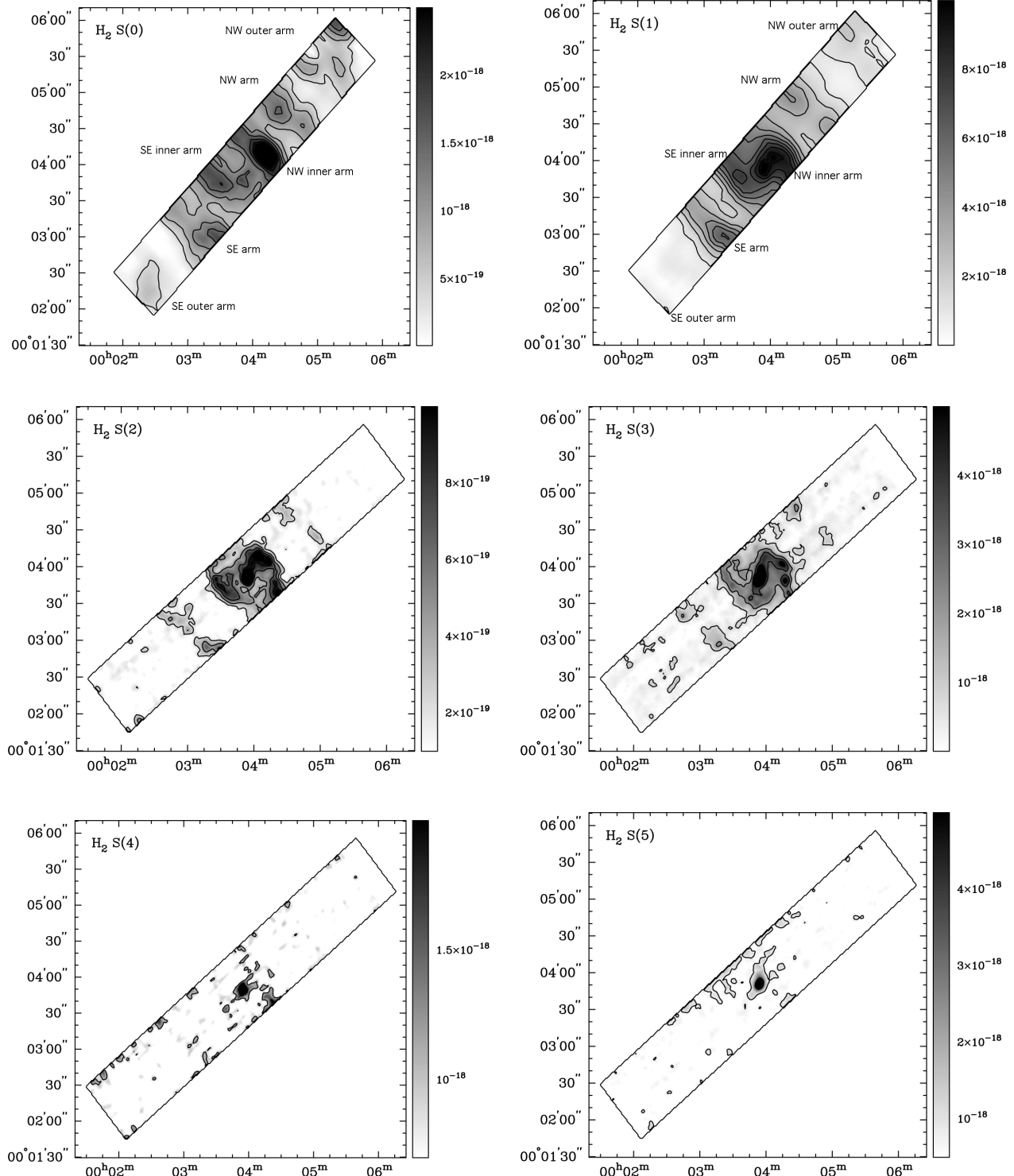


Fig. 1.— Maps of the H<sub>2</sub> S(0) (*top left*), H<sub>2</sub> S(1) (*top right*), H<sub>2</sub> S(2) (*middle left*), H<sub>2</sub> S(3) (*middle right*), H<sub>2</sub> S(4) (*bottom left*), and H<sub>2</sub> S(5) (*bottom right*) intensity across the SL and LL strips that we mapped with the Spitzer IRS. The H<sub>2</sub> S(0) and H<sub>2</sub> S(1) maps are created from the LL data cubes. The H<sub>2</sub> S(2), H<sub>2</sub> S(3), H<sub>2</sub> S(4), and H<sub>2</sub> S(5) maps are created from the SL data cube. The grey-scale is in units of W/m<sup>2</sup>. Contour levels are at  $2.9 \times 10^{-18}$ ,  $2.2 \times 10^{-18}$ ,  $1.8 \times 10^{-18}$ ,  $1.5 \times 10^{-18}$ ,  $1.1 \times 10^{-18}$ ,  $7.3 \times 10^{-19}$ , and  $3.7 \times 10^{-19}$  W/m<sup>2</sup> for H<sub>2</sub> S(0);  $9.6 \times 10^{-18}$ ,  $8.6 \times 10^{-18}$ ,  $7.5 \times 10^{-18}$ ,  $6.4 \times 10^{-18}$ ,  $5.4 \times 10^{-18}$ ,  $4.3 \times 10^{-18}$ ,  $3.2 \times 10^{-18}$ ,  $2.1 \times 10^{-18}$  and  $1.1 \times 10^{-18}$  W/m<sup>2</sup> for H<sub>2</sub> S(1);  $1.1 \times 10^{-18}$ ,  $8.9 \times 10^{-19}$ ,  $6.7 \times 10^{-19}$ ,  $4.4 \times 10^{-19}$ , and  $2.2 \times 10^{-19}$  W/m<sup>2</sup> for H<sub>2</sub> S(2);  $1.21 \times 10^{-17}$ ,  $9.4 \times 10^{-18}$ ,  $6.7 \times 10^{-18}$ ,  $4.0 \times 10^{-18}$ , and  $1.3 \times 10^{-18}$  W/m<sup>2</sup> for H<sub>2</sub> S(3);  $2.0 \times 10^{-18}$  and  $1.0 \times 10^{-18}$  W/m<sup>2</sup> for H<sub>2</sub> S(4);  $7.3 \times 10^{-18}$ ,  $4.0 \times 10^{-18}$ , and  $8.0 \times 10^{-19}$  W/m<sup>2</sup> for H<sub>2</sub> S(5). The vertical axis is the right ascension and the horizontal axis is the declination. Note that in all of the maps, north is up and east is to the left. The different spiral arm regions are labeled on the H<sub>2</sub> S(0) and H<sub>2</sub> S(1) maps in order to aid in discussing the molecular gas morphologies. The box around the intensity maps represents the SL or LL strip that we mapped.

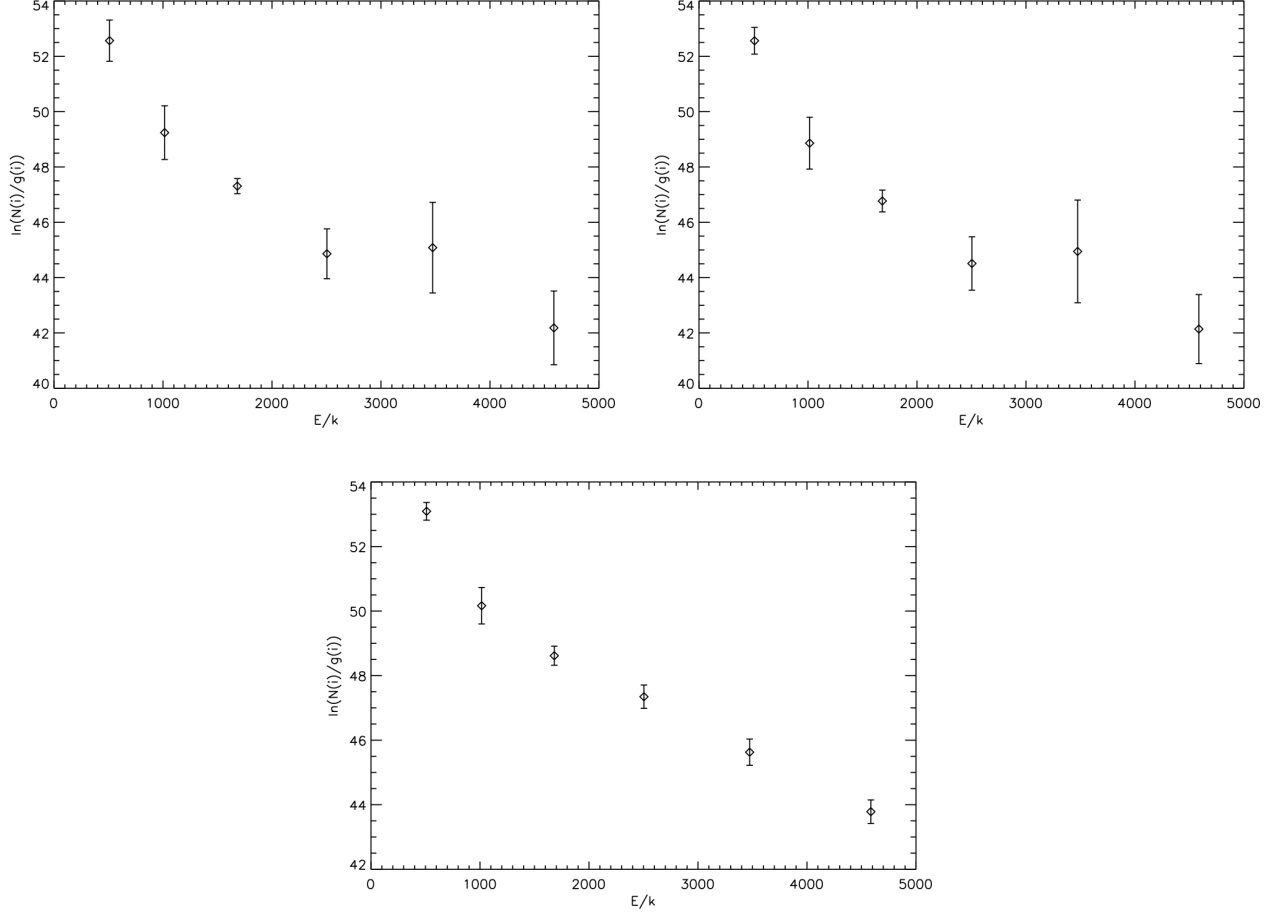


Fig. 2.— Excitation diagrams taken from 3 different regions along the M51 strip. The top two excitation diagrams are taken from regions within the southeast and northwest spiral arms that are  $10''.2$  in diameter ( $1.13 \times 10^5$  pc $^2$ ) and centered at (RA, Dec) of (202.45, 47.21) and (202.49, 47.18), respectively. The excitation diagram at the bottom is taken from the nuclear region. The aperture is  $10''.2$  in diameter ( $1.13 \times 10^5$  pc $^2$ ), centered at (RA, Dec) of (202.47, 47.19).

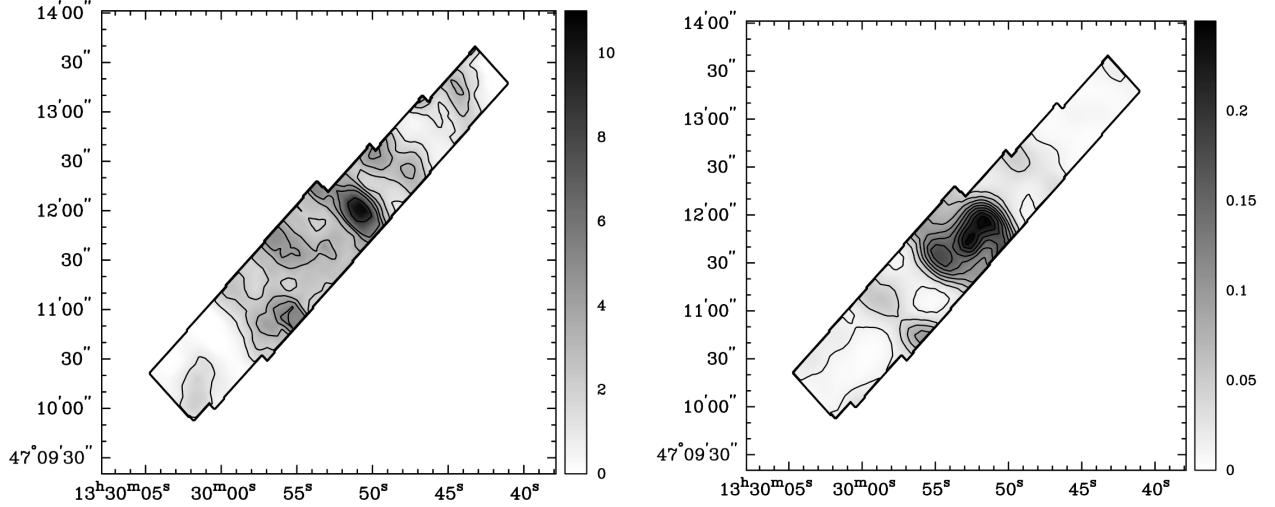


Fig. 3.— Shown are the warm ( $T = 100 - 300$  K)  $\text{H}_2$  (*left*) and hot ( $T = 400 - 1000$  K)  $\text{H}_2$  (*right*) mass distributions. The mass distributions are in units of  $M_{\odot}/\text{pc}^2$ . Contours are overplotted for clarity. The warm  $\text{H}_2$  mass contour levels are at 8.85, 5.55, 4.43, 3.32, 2.21, and  $1.10 M_{\odot}/\text{pc}^2$ . The hot  $\text{H}_2$  contour levels are at 10 % of  $0.25 M_{\odot}/\text{pc}^2$ . The hot  $\text{H}_2$  mass distribution is derived from the fit to the  $\text{H}_2 \text{ S}(2) - \text{H}_2 \text{ S}(5)$  lines and the warm  $\text{H}_2$  mass distribution is derived from the fit to the  $\text{H}_2 \text{ S}(0) - \text{H}_2 \text{ S}(2)$  lines, corrected for the contribution of the hot  $\text{H}_2$  mass phase.

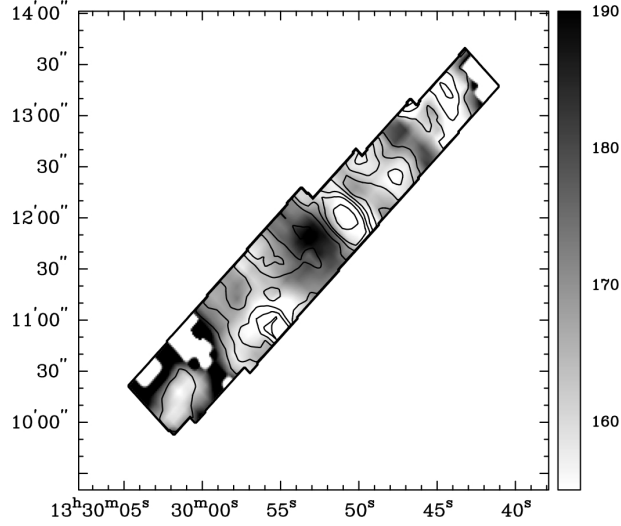


Fig. 4.— The warm ( $T = 100 - 300$  K)  $H_2$  mass distribution compared to the warm  $H_2$  excitation-temperature. The warm  $H_2$  excitation-temperature and mass distributions are derived from the fit to the excitation diagrams across the strip for the  $H_2$  S(0) –  $H_2$  S(2) lines, corrected for the contribution of the hot ( $T = 400 - 1000$  K)  $H_2$  phase. Mass density contour levels are at 8.85, 5.55, 4.43, 3.32, 2.21, and  $1.10 M_\odot/\text{pc}^2$  (same as in Figure 3). The grey-scale represents the excitation-temperature distribution (in units of Kelvin). The non-rectangular shape to the map is due to the slight offset of the *Spitzer* IRS SL strip relative to the LL strip.

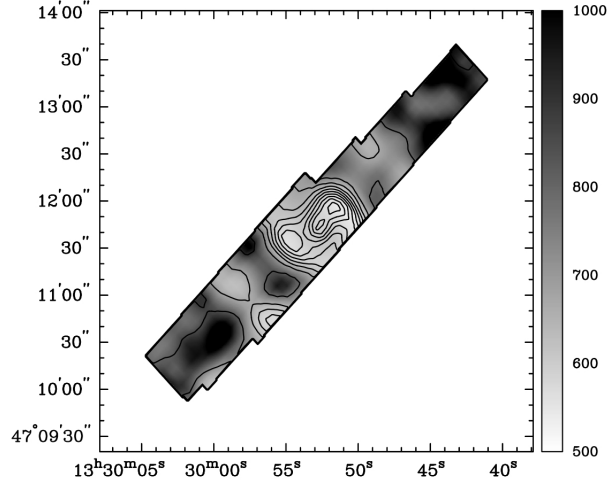


Fig. 5.— The hot ( $T = 400 - 1000$  K)  $H_2$  mass distribution compared to the hot  $H_2$  excitation-temperature. The hot  $H_2$  excitation-temperature and mass distributions are derived from the fit to the excitation diagrams across the strip for the  $H_2$  S(2) –  $H_2$  S(5) lines. Mass density contour levels are at 10% of  $0.25 M_\odot/\text{pc}^2$  (same as in Figure 3). The grey-scale represents the excitation-temperature distribution (in units of Kelvin).

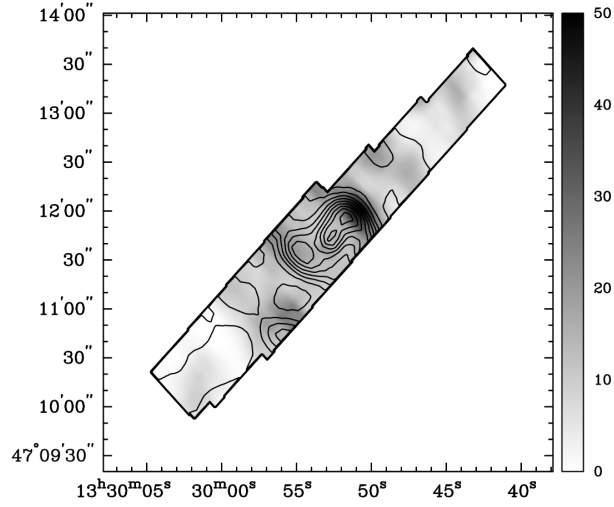


Fig. 6.— The warm ( $T = 100 - 300$  K)  $H_2$  mass (in grey-scale) compared to the hot ( $T = 400 - 1000$  K)  $H_2$  mass (in contours). Contours levels for the hot  $H_2$  mass distribution are at 10% of the maximum mass density  $0.25 M_{\odot}/pc^2$ . The grey-scale is in units of  $M_{\odot}/pc^2$ .

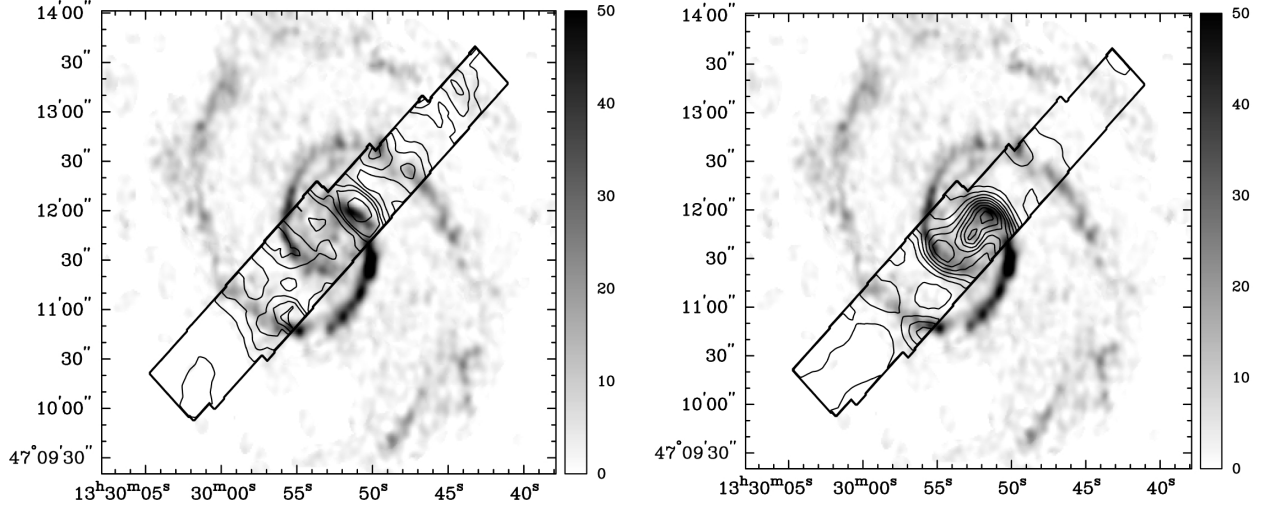


Fig. 7.— *Left:* Comparison of CO intensity (in grey-scale) to the warm ( $T = 100 - 300$  K) H<sub>2</sub> mass (in contours). The CO intensity is in units of Jy beam  $s^{-1}$ . The warm H<sub>2</sub> mass contours are the same as in Figures 3 and 4. *Right:* Comparison of CO intensity (in grey-scale) to the hot ( $T = 400 - 1000$  K) H<sub>2</sub> mass (in contours). The CO intensity is in units of Jy beam  $s^{-1}$ . The hot H<sub>2</sub> mass contours are the same as in Figures 3 and 5.

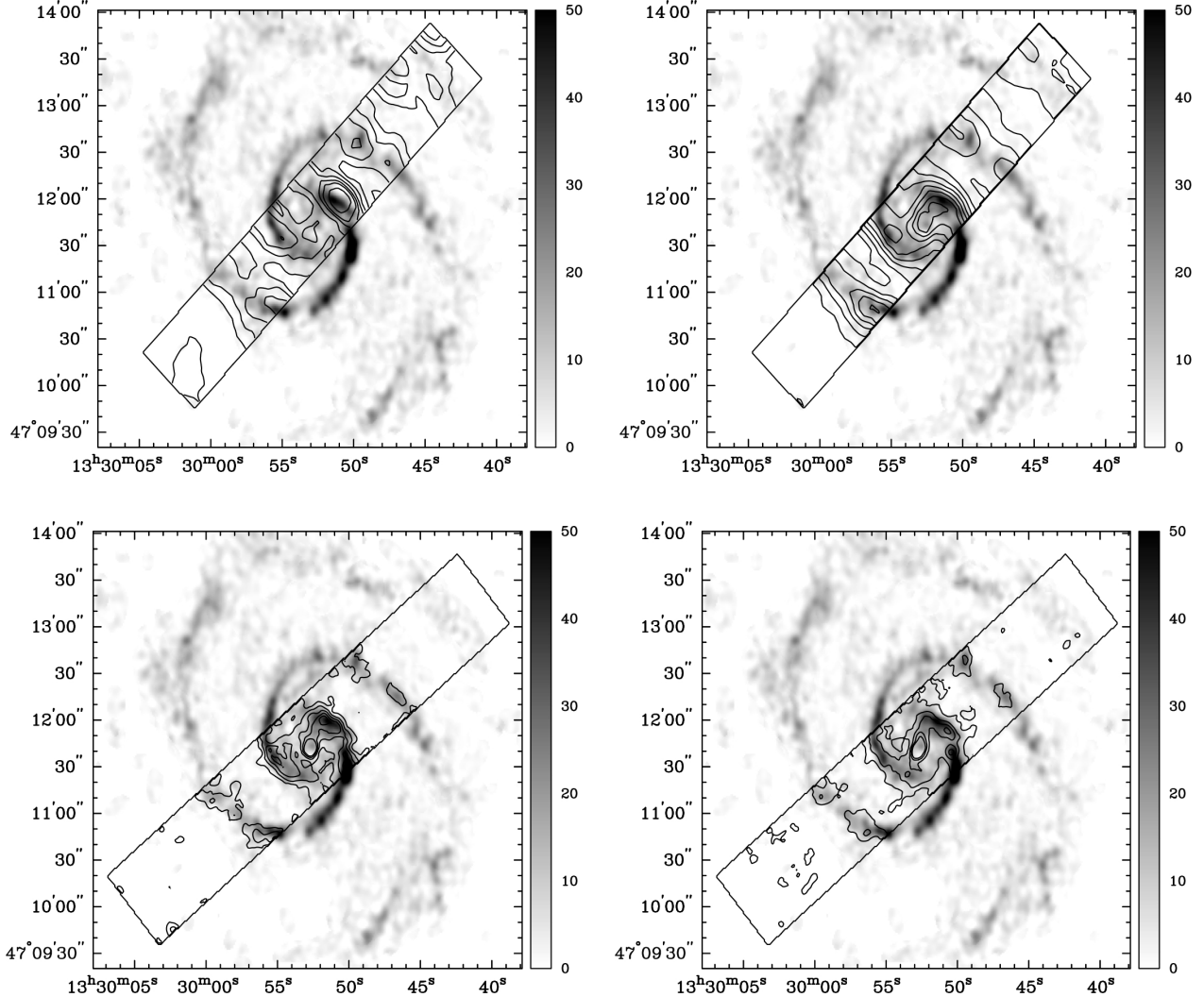


Fig. 8.— Comparison of the CO emission to the H<sub>2</sub> S(0) (*top left*), H<sub>2</sub> S(1) (*top right*), H<sub>2</sub> S(2) (*bottom left*), and H<sub>2</sub> S(3) (*bottom right*) emission. The CO emission maps are in units of Jy beam s<sup>-1</sup>. Contour levels for H<sub>2</sub> S(0), H<sub>2</sub> S(1), H<sub>2</sub> S(2), and H<sub>2</sub> S(3) are the same as in Figure 1.

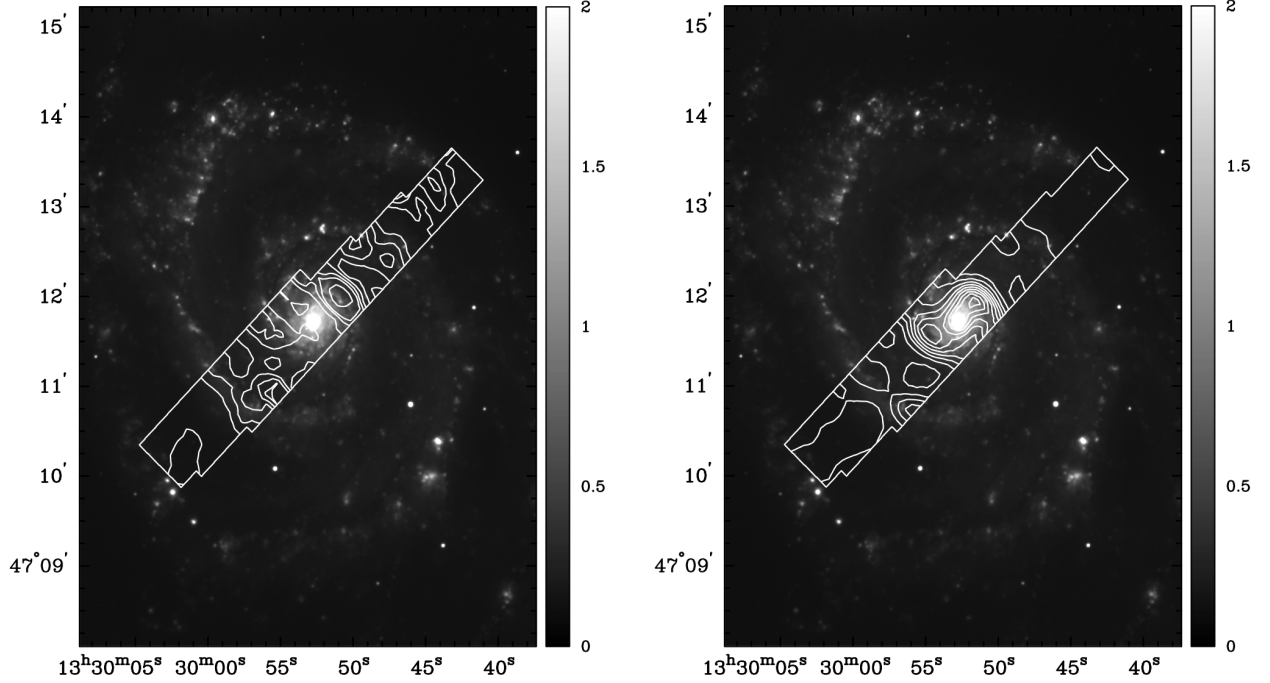


Fig. 9.— *Left:* Comparison of H $\alpha$  (in grey-scale) to the warm ( $T = 100 - 300$  K) H $_2$  mass (in contours). The H $\alpha$  image is in units of counts/sec. The warm H $_2$  mass contours are the same as in Figures 3 and 4. *Right:* Comparison of H $\alpha$  (in grey-scale) to the hot ( $T = 400 - 1000$  K) H $_2$  mass (in contours). The H $\alpha$  image is in units of counts/sec. The hot H $_2$  mass contours are the same as in Figures 3 and 5.

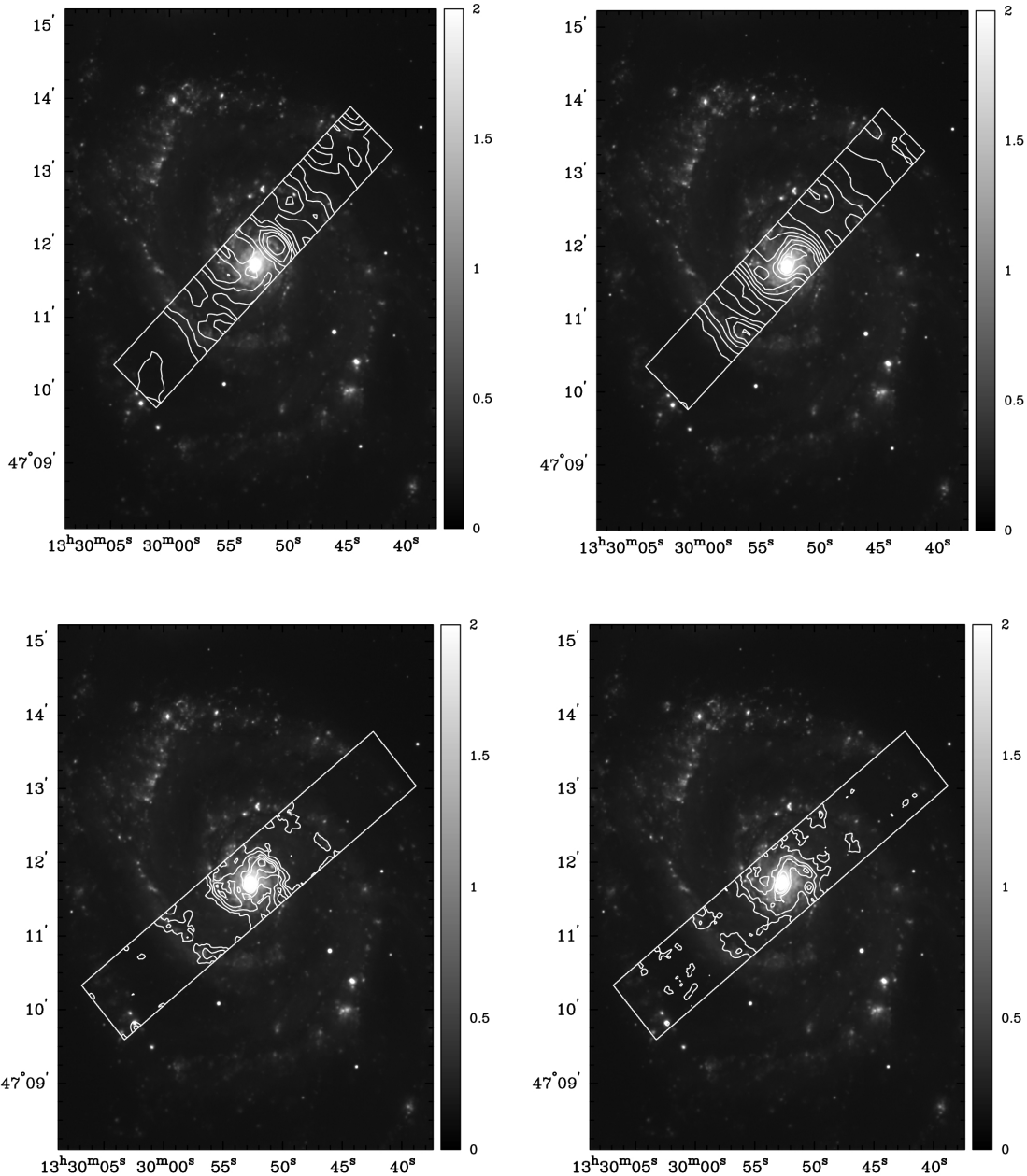


Fig. 10.— Comparison of H<sub>α</sub> emission to the H<sub>2</sub> S(0) (*top left*), H<sub>2</sub> S(1) (*top right*), H<sub>2</sub> S(2) (*bottom left*), and H<sub>2</sub> S(3) (*bottom right*) emission. The H<sub>α</sub> image is in units of counts/s. Contour levels for H<sub>2</sub> S(0), H<sub>2</sub> S(1), H<sub>2</sub> S(2), and H<sub>2</sub> S(3) are the same as in Figure 1.

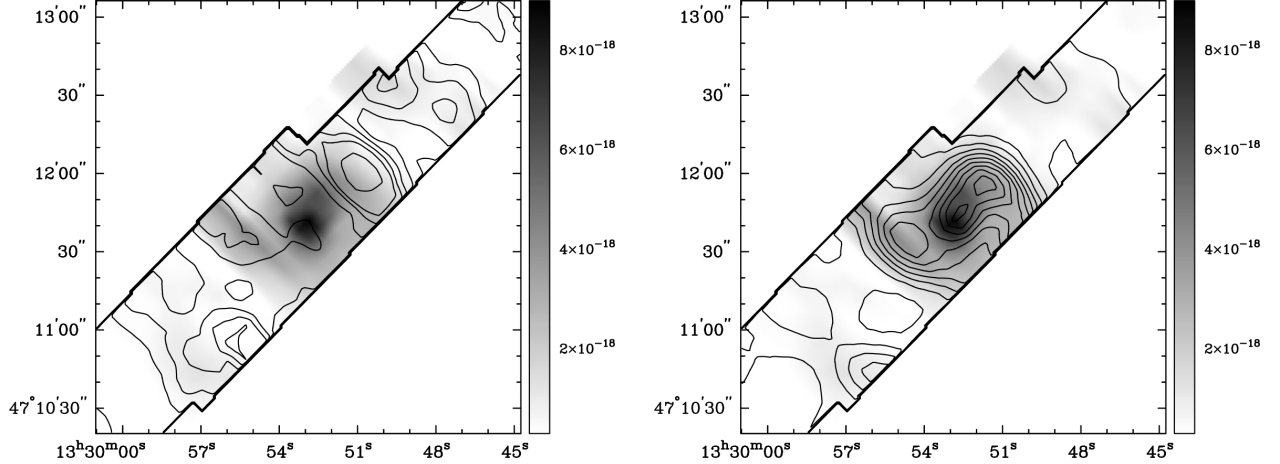


Fig. 11.— *Left:* Comparison of the [O IV](25.89  $\mu$ m) emission (in grey-scale) to the warm ( $T = 100$  K - 300 K) H<sub>2</sub> mass distribution (in contours). Hot H<sub>2</sub> mass contours are the same as in Figures 3 and 4. *Right:* Comparison of the [O IV](25.89  $\mu$ m) emission (in grey-scale) to the hot ( $T = 400$  - 1000 K) H<sub>2</sub> mass distribution (in contours). Hot H<sub>2</sub> mass contours are the same as in Figures 3 and 5. The [O IV](25.89  $\mu$ m) emission is in units of  $W/m^2$ .

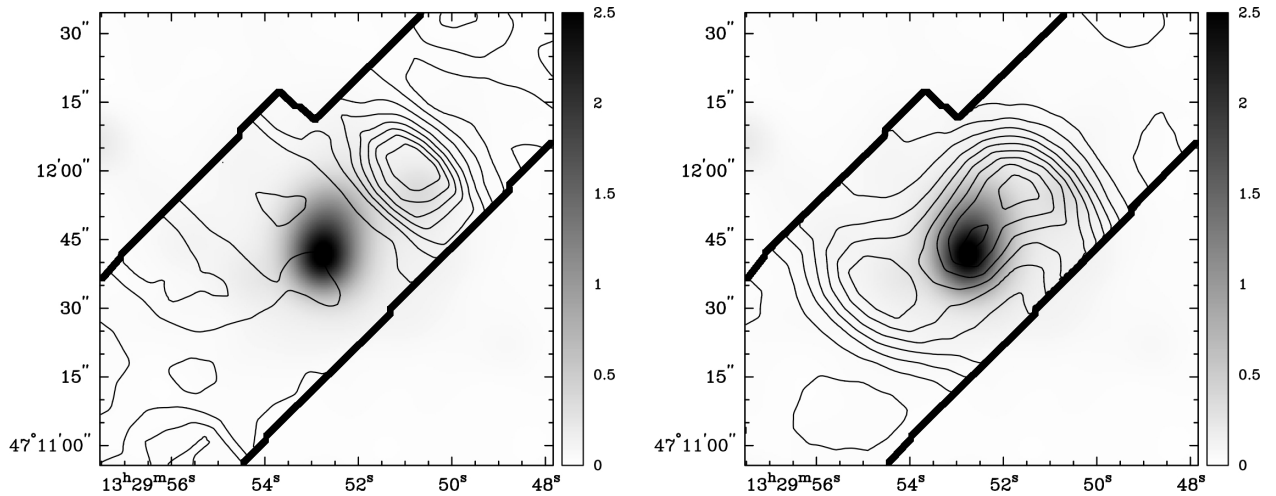


Fig. 12.— *Left:* Comparison of the smoothed 0.5 – 10 keV X-ray emission band (in grey-scale) to the warm ( $T = 100 - 300$  K)  $H_2$  mass distribution (in contours). The X-ray image has been smoothed to the same resolution as the warm  $H_2$  mass map. X-ray emission is in units of counts.  $H_2$  mass contours are the same as in Figures 3 and 4. *Right:* Comparison of the smoothed 0.5 – 10 keV X-ray emission band (in grey-scale) to the hot ( $T = 400 - 1000$  K)  $H_2$  mass distribution (in contours). The  $H_2$  mass distribution contours are the same as in Figures 3 and 5.

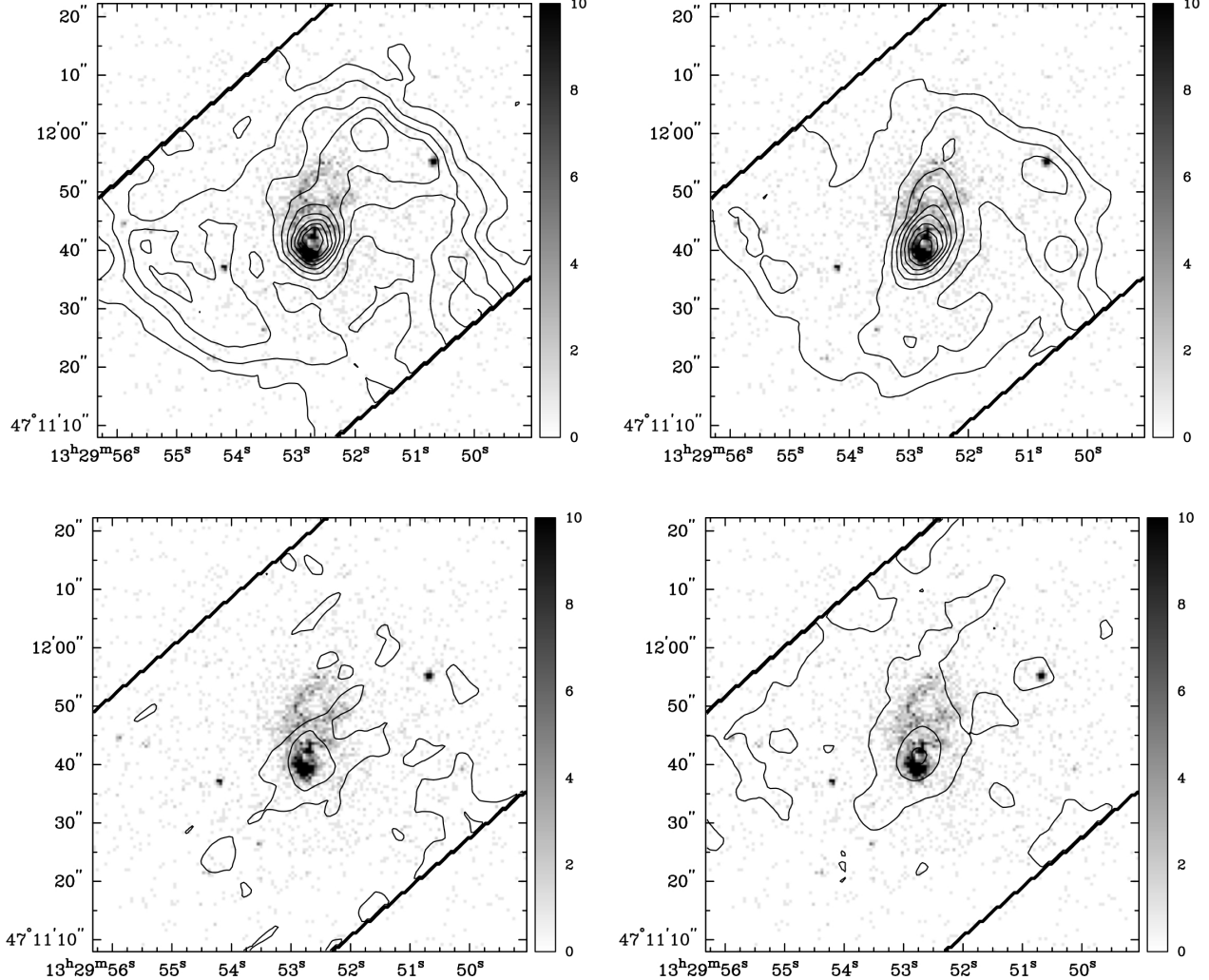


Fig. 13.— Comparison of the 0.5 – 10 keV X-ray emission band (in grey-scale) to the H<sub>2</sub> S(2) (*top left*), H<sub>2</sub> S(3) (*top right*), H<sub>2</sub> S(4) (*bottom left*), and H<sub>2</sub> S(5) (*bottom right*) emission in the nuclear region of M51. X-ray emission is in units of counts. The H<sub>2</sub> S(2) and H<sub>2</sub> S(3) emission contours are at 10 % of their peak values ( $2.20 \times 10^{-18}$  and  $1.35 \times 10^{-17}$  W/m<sup>2</sup>, respectively). The H<sub>2</sub> S(4) contours are at  $2.0 \times 10^{-18}$  and  $1.0 \times 10^{-18}$  W/m<sup>2</sup> and the H<sub>2</sub> S(5) contours are at  $7.3 \times 10^{-18}$ ,  $4.0 \times 10^{-18}$ , and  $8.0 \times 10^{-19}$  W/m<sup>2</sup>.

Table 1. H<sub>2</sub> Parameters

Transition	Wavelength ( $\mu\text{m}$ )	Rotational State (J)	Energy (E/k)	A (s $^{-1}$ )	Statistical Weight (g)
H <sub>2</sub> (0-0)S(0)	28.22	2	510	$2.94 \times 10^{-11}$	5
H <sub>2</sub> (0-0)S(1)	17.04	3	1015	$4.76 \times 10^{-10}$	21
H <sub>2</sub> (0-0)S(2)	12.28	4	1682	$2.76 \times 10^{-9}$	9
H <sub>2</sub> (0-0)S(3)	9.66	5	2504	$9.84 \times 10^{-9}$	33
H <sub>2</sub> (0-0)S(4)	8.03	6	3474	$2.64 \times 10^{-8}$	13
H <sub>2</sub> (0-0)S(5)	6.91	7	4586	$5.88 \times 10^{-8}$	45

Note. — The statistical weight (g) is  $(2J+1)(2I+1)$  where  $I$  equals 1 for odd J transitions (ortho transitions) and  $I$  equals 0 for even J transitions (para transitions).